

SPUDCAN HYDRODYNAMICS: ANALYSIS OF HYDRODYNAMIC COEFFICIENTS OF SPUDCANS IN PROXIMITY OF THE SEABED DURING JACK-UP INSTALLATION

R.S. Hoes

Delft University of Technology, The Netherlands

Email: reinoudsamuelhoes@gmail.com

Key words: *GustoMSC, Jack-up Installation Limits, Footing, Spudcan, Spudcan Impact Loads, Close to Seabed, Hydrodynamic Coefficients, Added mass, Damping, Drag, Model Tests, Forced Heave Oscillation*

Abstract

This thesis researches the change of the hydrodynamics of jack-up spudcans close to the seabed and the influence of this change on calculated jack-up motions. Two GustoMSC jack-up designs are selected as typical: a large drilling jack-up (CJ-70), and a small wind turbine installation vessel (NG-2500X). Limits for allowable wave heights during jack-up installation are determined by factors including station keeping and wave loading. Spudcan impact loading is an additional factor that becomes governing in long period waves. A better understanding of jack-up motions during installation can improve impact prediction methods and this could result in more favorable installation limits. Forced heave oscillation tests have been done at decreasing distances from a towing tank bottom with a skirted spudcan and a hexagonal spudcan. A thin disk was used to validate the model tests. Added mass of both models was found to increase with decreasing distance to seabed and with increasing amplitude. Quadratic heave damping was found to increase with decreasing distance to seabed. The latter was significantly larger for the skirted spudcan. Static frequency domain analyses were done with WAMIT and in-house GustoMSC software to investigate the influence of the measured increase of added mass and damping on the motions of typical jack-up's during installation. Spudcan motions of the CJ-70 showed significant decrease in long period waves. The spudcan motions of the NG-2500X showed a small decrease in sea states with long period waves. The decrease of CJ-70 motions could improve installation limits in these conditions. Further research is however needed to analyze neglected effects and to quantify the improvement in installation limits for drilling jack-up's with skirted spudcans. The decrease of NG-2500X motions is considered to be not significant enough, to indicate a possible improvement in installation limits for small wind turbine installation vessels, with hexagonal spudcans.

1. Introduction

Jack-up's are self-installing working platforms used for a variety of applications, including drilling purposes and wind turbine installation. A jack-up consists of a floating hull with multiple retractable legs. Once floated to location with the legs pulled up, the legs can be lowered to the seabed. After the legs have landed on the seabed, the hull can be elevated above the water. The lower tip of the jack-up leg has to provide a firm connection with the seabed to support the entire weight of the vessel under environmental loading. For this purpose, the legs are often equipped with spudcans (footings) to increase the soil bearing area of the leg. Two GustoMSC jack-up designs, that are commonly used in the offshore industry, have been selected as typical designs. The CJ-70 design represents the drilling sector and the NG-2500X design represents the wind turbine installation vessels. The spudcan types that are used for the CJ-70 and NG-2500X have been selected as typical spudcan designs: large skirted spudcans and small hexagonal spudcans, respectively.

Jack-up installation consists of several steps. Before the jack-up is installed, it floats above the desired location on its own account. It stays on this location using tugs or dynamic positioning (DP) systems. The legs are then lowered by means of the jacking system. Until the footings touch the seabed, the platform remains afloat

and still moves due to surface waves. After the spudcans have touched down on the seabed, ballast water is taken in during the preloading. This ensures that the spudcans settle firmly into the soil and will not penetrate the seabed any further during operation. Subsequently the rig is jacked out of the water to create an air gap high enough to avoid waves hitting the hull.

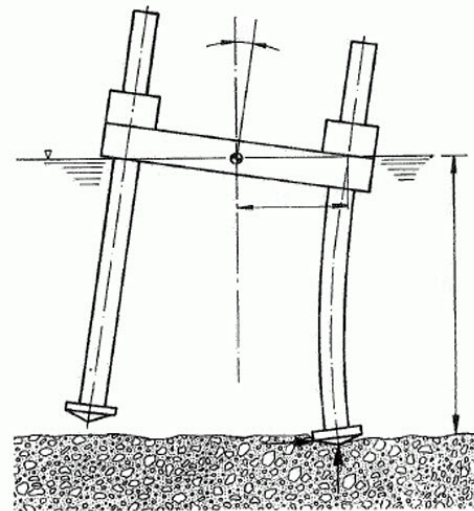


Figure 1: Simplified spudcan impact model, DNV [2012]

Classification societies such as DNV [2012] demand limiting environmental siting conditions to be specified by the designer. The practical limit for significant wave

heights during installation lies around $H_s = 1.0 - 2.0[m]$ and is determined by factors including station keeping, green water and wave loading during pre-loading. Spudcan impact loading is an additional factor that has to be taken into account. As the jack-up does not yet have a fixed connection with the seabed, waves will cause heave, pitch and roll motions of the hull, which are translated to surge, sway and heave motions of the spudcans. As the legs are lowered, the spudcans eventually impact the seabed (figure 1). During this touch-down phase, impacts impose loads on the spudcans, legs and the leg/hull interface, which can lead to damage. High impact loads are caused by large hull motions, and impact loading generally becomes governing over the practical limit in long period waves (i.e. wave spectra with high peak periods, T_p). Figure 2 shows that the impact loading can halve the installation limit in these conditions.

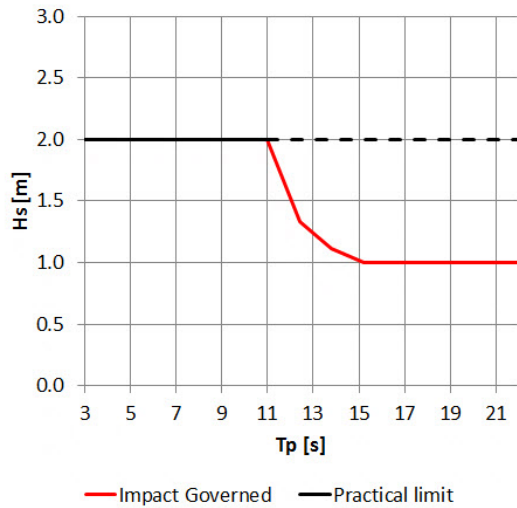


Figure 2: Example of installation limit: allowable significant wave heights versus peak periods of wave spectra

The height of spudcan impact loads is dependent on a number of factors, including soil characteristics and impact velocity of the spudcans. The latter follows from the jack-up and spudcan motions, so a better understanding of the factors influencing these motions during installation could improve impact prediction methods. Literature indicates that hydrodynamic heave coefficients of an object change when it gets closer than $1/2$ times its diameter to the seabed (e.g. Brennen [1982], Garrido-mendoza et al. [2013]) and it can be expected that this is also true for spudcans. The state-of-the-art methods that simulate spudcan impacts to determine limiting environmental installation conditions, do not consider such a change of spudcan hydrodynamics. The objective of this thesis is to improve the certainty of the prediction of spudcan impact loads. This has been done by analyzing the change of the hydrodynamics of spudcans moving close to a seabed and investigating the influence of this change on the calculated jack-up and spudcan motions.

¹Since the spudcan is submerged, no damping due to wave generating will occur.

2. Hydrodynamics of Spudcans

To evaluate the hydrodynamic properties of a spudcan when it approaches the seabed, it is viewed as an individual submerged object in forced oscillation, shown in figure 3. The forced motions are imposed by the jack-up vessel via the leg connected. Motions of the Centre of Gravity (CoG) of a jack-up in six Degrees of Freedom (DoF) will cause spudcan motions in predominantly heave, sway and surge direction (Chakrabarti [2012]). Considering the typical flat shape of spudcans, sway and surge added mass and damping¹ are expected to be small compared to heave. Therefore the heave motion is assumed to be of most interest for the purpose of determining the effects of seabed proximity on spudcan hydrodynamics.

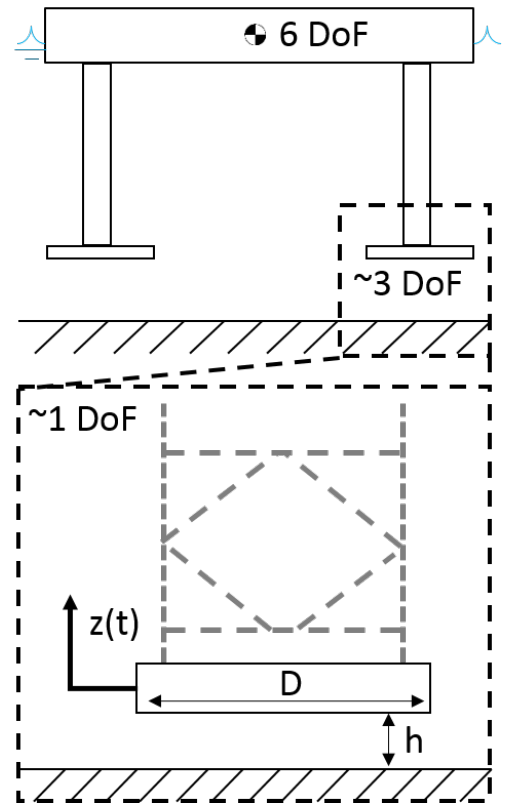


Figure 3: Simplified spudcan motion model

In heave direction, a typical spudcan is approximately axis-symmetrical. Therefore, the spudcan heave motion can be assumed decoupled from other motions. It is assumed that in regular waves the vertical motion of the spudcan caused by the motions of the jack-up can be expressed as sinusoidal motion. If decoupled, the heave motion of submerged oscillating objects with small amplitude can be expressed by equation 1 (Roe [2008]). The source of F_D can be considered as drag, which is proportional to the velocity squared, similar to Morison's equation, given by equation 2 (Tao and Dray [2008], Sarpkaya and Isaacson [1981]).

$$F(t) = (M + A)\ddot{z} + F_D(\dot{z}) \quad (1)$$

$$F_D(\dot{z}) = \frac{1}{2} * \rho * S * C_d * \dot{z}(t) |\dot{z}(t)| \quad (2)$$

When the damping is linearized, it can be rewritten as equation 3 and using fourier decomposition, the linear damping coefficient B can be written as equation 4 (Tao and Dray [2008], Sarpkaya and Isaacson [1981]). Equation 6 is the Keulegan-Carpenter number, which is a non-dimensional representation of the oscillation amplitude.

$$F_D(\dot{z}) \approx B\dot{z}(t) \quad (3)$$

$$B = \frac{1}{3} \mu \beta D KC C_d \quad (4)$$

With:

$$\beta = \frac{D^2 f}{\nu} \quad (5)$$

$$KC = \frac{2\pi z_0}{D} \quad (6)$$

In deep water, the heave added mass can be derived with potential theory. When approximating a spudcan as a thin solid circular disk with radius r , the added mass is given by equation 7 (Lamb [1932], Sarpkaya and Isaacson [1981]). It is used to non-dimensionalize spudcan added mass A to C_a , as shown by equation 8 (Wadhwa [2010]).

$$A_{disk} = \frac{8}{3} \rho r^3 \quad (7)$$

$$C_a = \frac{A}{A_{disk}} = \frac{A}{\frac{8}{3} \rho r^3} \quad (8)$$

The linear damping coefficient B is non-dimensionalized to the linear damping coefficient C_b by equation 9 (Wadhwa [2010]). It can be rewritten as the drag coefficient C_d , according to equation 10 (Tao and Dray [2008], Garrido-mendoza et al. [2013]).

$$C_b = \frac{B}{2\omega A_{disk}} \quad (9)$$

$$C_d = \frac{C_b 4\pi}{KC} \quad (10)$$

A review of several studies regarding submerged objects oscillating in heave with small amplitudes, is given below:

- Inertia forces are dominant over drag forces for low KC. With higher KC, drag force due to flow separation becomes more important (He et al. [2008]).
- KC number has large influence on both C_a and C_b (Tao and Dray [2008], Wadhwa [2010], Garrido-mendoza et al. [2013]).
- Aspect ratio $\frac{t}{D}$, ratio between thickness and diameter, has influence on vortex shedding around sharp edges of an object. This subsequently influences C_b and C_d (Tao and Thiagarajan [2003b], Tao and Thiagarajan [2003a]).

- The frequency of oscillation doesn't a large effect on hydrodynamic coefficients of thin plates (Wadhwa [2010], Li et al. [2013]), nor a suction can (Ireland [2007]). In region $KC \approx 0.1 - 2.0$ and $Re > 1 * 10^3$, flow separation occurs at sharp edges of spudcans and Froude scaling can be applied: separation results in low friction drag and high pressure drag. This indicates low dependence on viscosity or Re (Hoerner [1965], He et al. [2008]).
- C_a , C_b and C_d increase as an object approaches a solid seabed (Brennen [1982], Molin et al. [1999], Garrido-mendoza et al. [2013]).
- Increase in C_a originates from high fluid velocities between object and seabed and pressure differences (Brennen [1982]), whereas the increase of damping coefficients seems to be dependent on changes in vortex shedding due to vortex interaction with nearby seabed (Garrido-mendoza et al. [2013], Garrido-Mendoza and Thiagarajan [2014]).
- Potential theory indicates that close to the seabed a 'slamming' term, proportional to velocity squared, influences the hydrodynamic forces on a heaving spudcan (Brennen [1982], Molin et al. [1999], Nielsen and Statoil [2007]).
- Diffraction programs like WAMIT can estimate C_a near the seabed at low KC numbers, $KC < 0.2$ (Nielsen and Statoil [2007]).
- Hydrodynamic soil behavior (Wadhwa [2010]), in-plane/sideways flow (Yang et al. [2013]) and spudcan porosity (Tao and Dray [2008]) are other possible influences on C_a , C_b and C_d .

3. Forced oscillation tests

Forced heave oscillation tests were done to analyze C_a , C_b and C_d of spudcans when approaching the seabed. The tested models, shown by figure 4, represent the spudcans of typical jack-up's: a skirted spudcan (CJ-70) and a hexagonal spudcan (NG-2500X). A thin disk was used to validate the model tests with previous results from literature (Wadhwa [2010], Garrido-mendoza et al. [2013]).

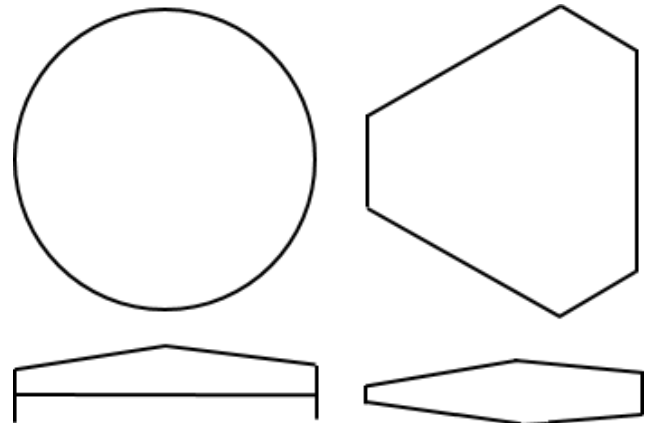


Figure 4: Models, left: CJ-70, right: NG-2500X

Table 1: Test Matrix

Parameters	Models	NG, CJ, Disk
Model diameter [mm]		200
Model weight (incl. equip.)[kg]		2.3, 2.7, 2.2
Equivalent full scale D [m]		6.1, 10, 22
Scale factors		30.5, 110, 160
Oscillation direction		Heave
Dist. seabed[h/D]		0.05, 0.10, 0.25, 0.5, 1.0
Dist. seabed[mm]		10, 20, 50, 100, 200
Keulegan-Carpenter no.		0.09 - 1.45
Model amplitudes [mm]		3 - 46
Gap heights [mm]		3 - 154
Full scale Freq.[rad/s]		0.4 - 0.6/1.1
Model Freq.[rad/s]		2.2 - 6.3
Angle [deg]		0, 1.5, 3

A uni-axial oscillator (Mavilor Iberica, 600-324) was mounted on the towing carriage and used to oscillate spudcans in heave direction at several distances, h/D (dimensionless), from the bottom of DUT towing tank No. 2 (Figure 6; Length = 85.0[m], Width = 2.75[m], Water depth ≈ 0.70 [m], Bottom roughness ≈ 0.4 [mm]), as shown by figure 5. Table 1 gives an overview of the test parameters. The following assumptions/simplifications are made with regard to the forced oscillation tests:

- Seabed is modeled as horizontal, smooth, rigid and impenetrable. Spudcans are oscillated above smoothed area (Peters and Huijsmans [2011]).
- Change in C_a , C_b and C_d as function of h/D in directions other than heave is negligible.
- Heave excitation is caused by roll and pitch of the hull: frequency of interest is in region of roll and pitch natural frequency of the entire jack-up. Roll and pitch cause a max. spudcan inclination of 3°.
- Legs do not have a significant influence on the change of C_a , C_b and C_d
- Flow separation takes place at low Reynolds numbers (Re), and Froude scaling laws can be used.

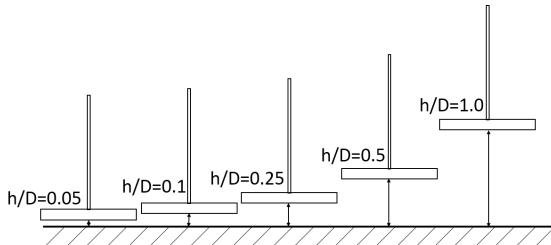


Figure 5: Non dimensional distance to seabed

Figure 7 schematically shows the method used to analyze C_a , C_b and C_d in the heave direction. Vertical displacement is measured with a linear motion potentiometer (ELAP PL231 200, uncert: 0.1[mm]), fixed to the side of the oscillator. At the moving end of the oscillator a 50 [N] load cell (DUT design: SB MR 047.5 and SB MR 047.5 II, uncert: 0.1[N]) is placed, to measure the heave response force. During the tests, possible waves in the

tank are measured with a resistance type wave-height probe (DUT; range: 400 [mm]). A height adjustable, hollow, RVS rod filled with polyurethane foam (outer diameter: 20 [mm], inner diameter: 16 [mm], total length: 928 [mm]) connected load cell and spudcan.

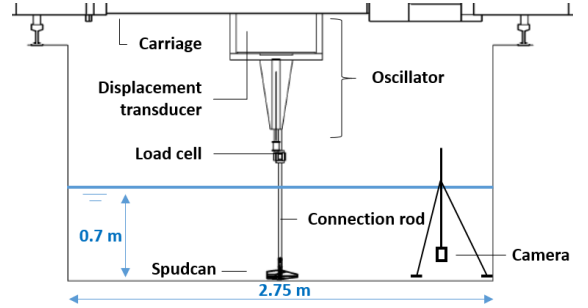


Figure 6: test setup

After amplification, all signals are filtered from 2000 [Hz] to 200 [Hz]. Signals are then processed with NIDAQ 18.8 measurement software. Using the first order Fourier fit function in MATLAB (R2014b), amplitude, frequency and phase of force and position signal are determined.

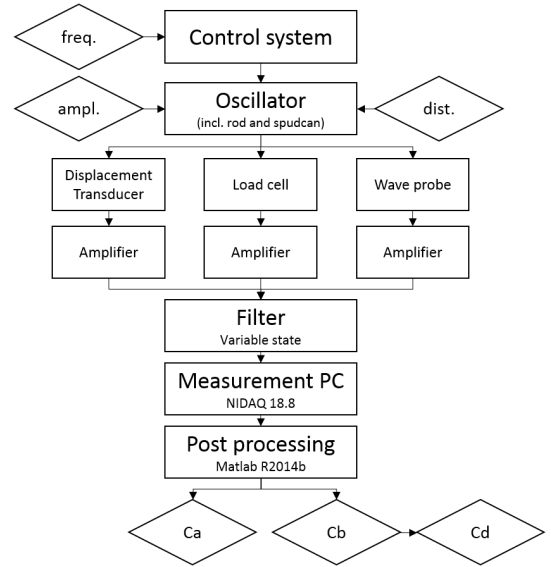


Figure 7: workflow

The phase difference between the force and the position can then be used to decompose force into an in-phase and out-of-phase component. This produces acceleration and velocity proportional quantities defined as added mass and linearized damping, given by equations 11 and 12, where z_0 and F_0 are the magnitudes of displacement and force, respectively. ϕ is the phase difference between the signals.

$$A = \frac{F_0 \cos(\phi) - C z_0}{-(z_0 \omega^2)} - M \quad (11)$$

$$B = \frac{F_0 \sin(\phi)}{(z_0 \omega)} \quad (12)$$

Figure 8 shows an example of a position and force time trace from which the added mass and damping are obtained. It can be seen that the oscillator produces a sinusoidal position signal. The measured force-time traces have a largely sinusoidal shape at high $\frac{h}{D}$ and low KC , when the noise is filtered by Fourier analysis (Noise is however assumed to introduce high uncertainty at low forces, $F < 0.5[N]$). With increasing KC (dependent on $\frac{h}{D}$), force trace deviates from the sinusoidal shape. This can be linked to critical KC mentioned by Wadhwa [2010] and Garrido-mendoza et al. [2013]. The non-sinusoidal shape could be caused by differences between values of C_d and C_a at the top of an oscillation stroke and the bottom of a stroke².

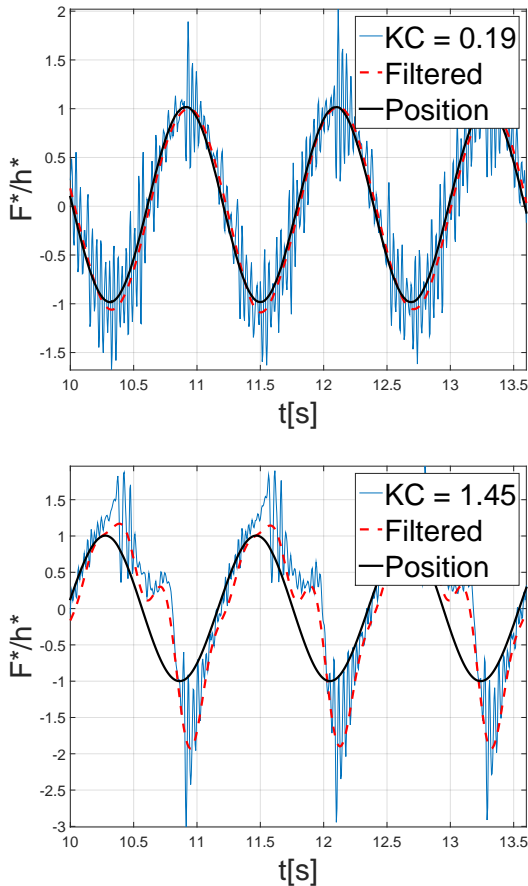


Figure 8: Example of force and displacement signals, sinusoidal and non-sinusoidal (normalized: h/h , $F/(h * \omega^2)$). CJ-70, $\frac{h}{D} = 0.25$, $\omega = 5.3[rad/s]$.

The effect is more pronounced for the disk and CJ-70 than for the NG-2500X, possibly because the increase of C_d with decreasing $\frac{h}{D}$ is much larger for the first. The used fitting method requires a sinusoidal force trace, and hydrodynamic coefficients derived from non-sinusoidal force traces are considered unreliable (indicated by dot-

ted lines in the graphs)³. Figure 9 shows that the results for the disk are in good agreement with literature (also true for other heights, which are not shown). The differences with Wadhwa [2010] are assumed to be because the bottom consisted of porous loose sand. The agreement is good enough to assume the results of the other spudcans are also valid.

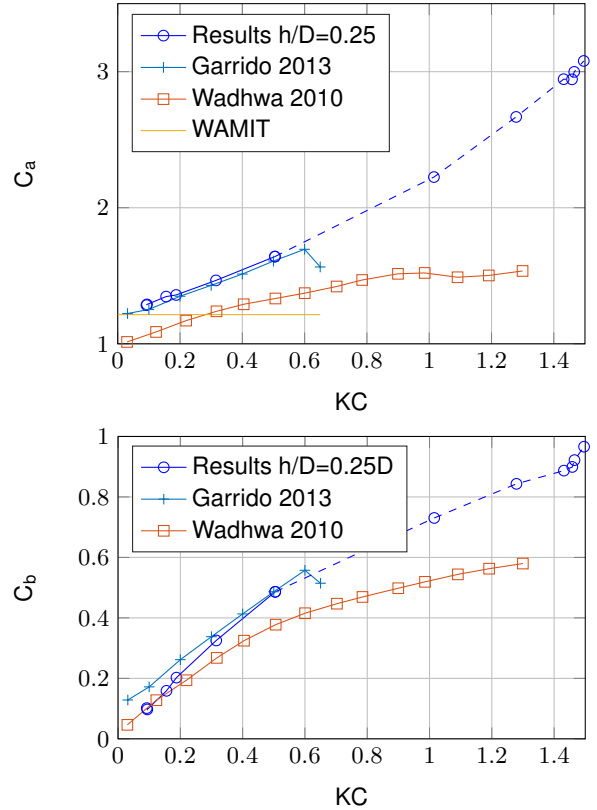


Figure 9: Test results disk C_a and C_b versus KC compared with literature, $\frac{h}{D} = 0.25$, $\omega = 6.4rad/s$. Dotted line indicates low quality fitting

Figures 10 and 11 show measured C_a and C_d versus KC for CJ-70 and NG-2500X, respectively. Figure 12 shows C_a and C_d versus $\frac{h}{D}$ at low KC . For all tested spudcans, C_a is dependent on both KC and $\frac{h}{D}$. C_a increases with decreasing $\frac{h}{D}$. At $\frac{h}{D} = 0.5$, C_a approximately equals the deep water value. There, the CJ-70 spudcan has the highest C_a , caused by the water entrapped between the skirts. The C_a calculated by WAMIT (potential theory) compares well with the model tests for all spudcans at low KC . The C_a for all spudcans in general has a positive dependence on KC . The negative KC dependence of CJ-70 C_a at $\frac{h}{D} = 0.1$ and 0.05 cannot be readily explained but it might be caused by the influence of other factors or harmonics. The break in trend at $\frac{h}{D} = 0.25$ could be caused by issues with the fitting of the non-sinusoidal shaped force-time trace.

²Empirical relations for the hydrodynamic coefficients, that were determined from the test results, showed to give a fair reconstruction of the measured forces, when implemented in an equation of motion.

³Visual evaluation of the fits led to the criterion that if $RMSE/F_0 > 0.1$ (Root Mean Squared Error, see MathWorks [2015]), a fit is rejected.

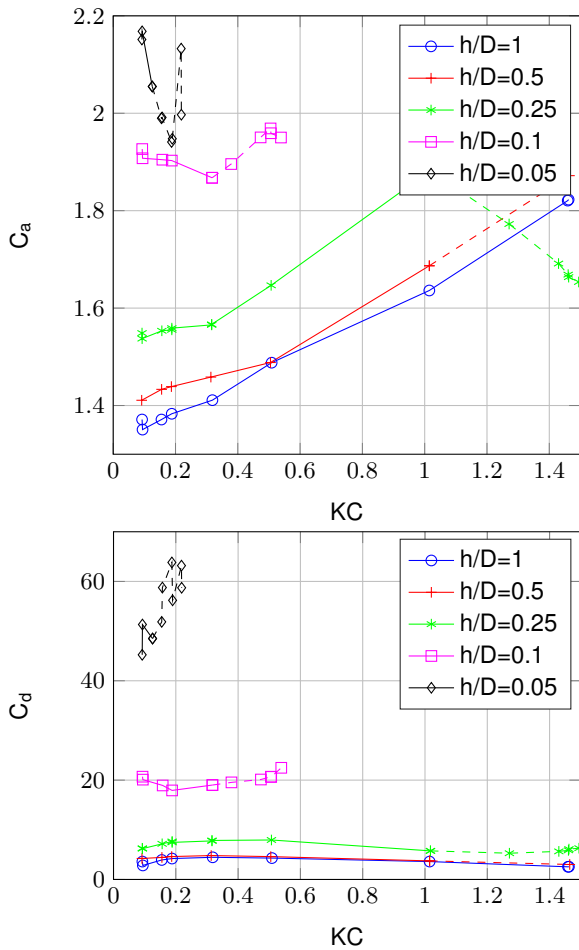


Figure 10: Test results CJ-70 C_a and C_d versus KC at varying distances to bottom. $\omega = 5.3rad/s$. Dotted line indicates low quality fitting.

The drag coefficient C_d for all spudcans approximately equals the deep water value at $\frac{h}{D} = 0.5$, and shows an increase with decreasing $\frac{h}{D}$. It shows negligible dependence on KC for CJ-70 and a slight positive dependence for NG-2500X. That behavior can be explained as consistent with Li et al. [2013], who gives a changing KC dependence of C_d with changing aspect ratio ($\frac{t}{D}$). C_d is larger for the CJ-70 spudcan than for the NG-2500X, which could be explained by the more streamlined shape of the latter and differences in vortex shedding regimes.

Furthermore (not shown), the dependence of C_a and C_d on oscillation frequency is found to be negligible for all three spudcans (it is assumed that observed differences between NG-2500X C_d for different frequencies at low KC , are caused by high uncertainty due to high noise at low forces). Influence of oscillation under an angle up to 3 degrees on C_a and C_d is also negligible.

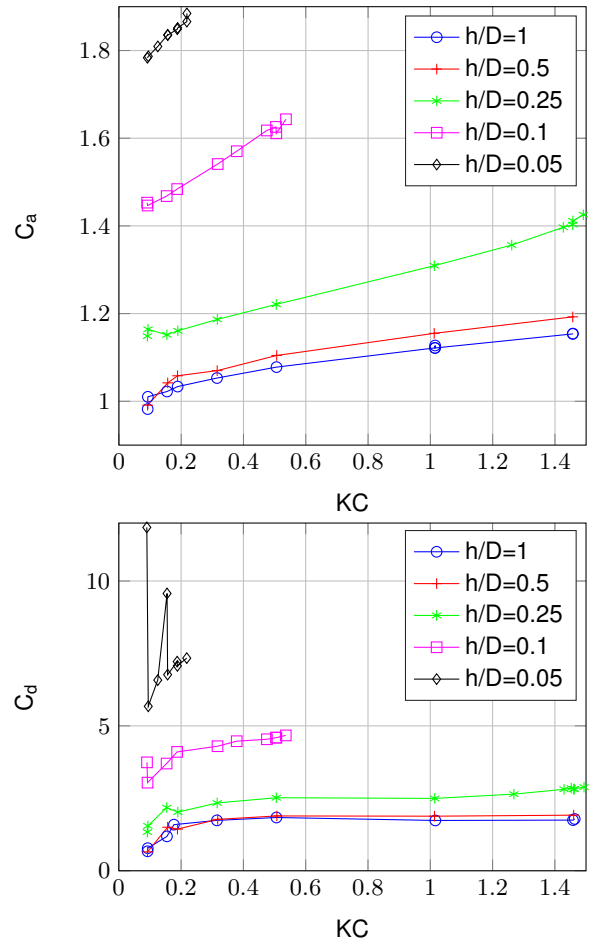


Figure 11: Test results NG-2500X C_a and C_d versus KC at varying distances to bottom. $\omega = 6.4rad/s$.

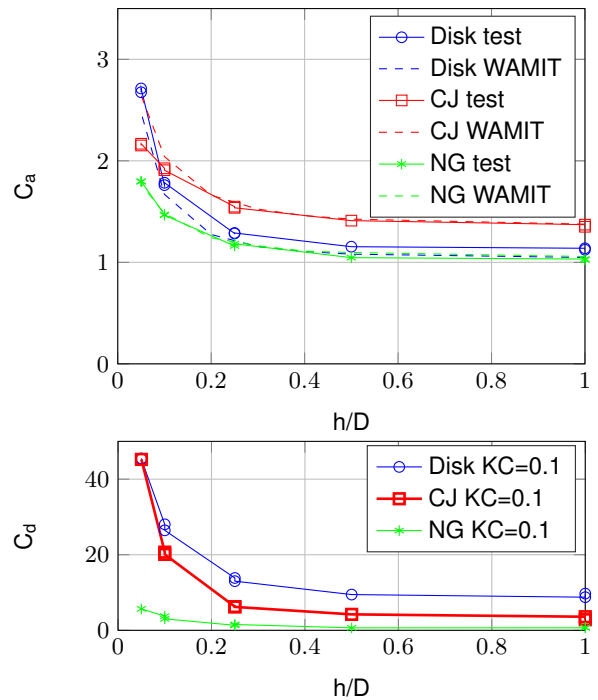


Figure 12: C_a and C_d versus $\frac{h}{D}$. $\omega = 6.4rad/s$, $KC \approx 0.1$

4. Jack-up motions

To investigate the influence of the measured increase of spudcan heave C_a and C_d on motions of typical jack-up's during installation, the motions of the typical jack-up designs are analyzed with static frequency domain analyses. For two water depths, each jack-up design is stationary analyzed with distances between spudcans and the seabed of $\frac{h}{D} = 0.5, 0.25, 0.1$ and 0.05 . The spudcan heave C_a and C_d are set to the values that were measured in the forced oscillation tests. The following additional assumptions/simplifications are made:

- The relation between wave height and motion response can be linearized for a given wave height.
- Existing GustoMSC models are a state-of-the-art and give a fair representation of reality (the models are validated with in-house model test data).
- The influence of KC (heave amplitude) on the spudcan heave coefficients, C_a and C_d , can be neglected.
- WAMIT correctly calculates the added mass of the typical jack-up models including the spudcan, i.e. WAMIT approximates the spudcan heave C_a as measured.

The analysis procedure consists of three steps. First, a 3D panel model⁴ of the jack-up is used as input for the diffraction panel program WAMIT, that calculates the wave forces, radiation forces (added-mass and potential damping) and restoring forces. Then, these results are combined with mass properties and Morison's drag elements and used as input for the in-house GustoMSC software CALMOT. This program solves the equation of motion of the jack-up in the frequency domain to generate the response in regular waves. The viscous drag is related to the velocity squared but is linearized for a given wave height, in order to obtain the responses in the frequency domain. The 6-DoF equation of motion is given by equation 13. Where the inertia matrix $[M + A]$ follows from WAMIT and mass properties, coefficient matrices $[B_{pot}]$ and $[C]$ follow from WAMIT and $[B_{visclin}]$ matrix follows from linearized Morison's elements on the hull, legs and spudcans. CALMOT also transforms the origin of the calculated motions to the CoG and the spudcans. Table 2 gives an overview of the analysis parameters. The panel models are shown by figure 13.

$$[M + A][\ddot{u}(t)] + [B_{pot}][\dot{u}(t)] + [B_{visclin}][\dot{u}(t)] + [C][u(t)] = [F(t)] \quad (13)$$

The last step is a spectral analysis to translate the RAO's to significant motion amplitudes in a given sea state. Standard single peaked Pierson-Moskowitz (PM) spectra are used for this analysis because the chance is significant that the sea state during jack-up installation is fully

developed. Wind waves (low T_p) and swell (high T_p) are considered separately.

Table 2: Analysis matrix. *WAMIT approximates the values of C_a for the spudcan heave motions.

	CJ-70		NG-2500X	
	Ca*	Cd	Ca*	Cd
h/D [-]				
0.5	1.4	3	1.1	1.8
0.25	1.5	7	1.2	3
0.1	1.9	20	1.4	5
0.05	2.2	47	1.7	8
Waterdepth [m]	120, 150		45, 60	
Headings [deg]	0 - 180		0 - 180	
Wave freq. [rad/s]	0.1 - 2.0		0.1 - 2.0	
Spectrum	PM		PM	
T_p [s]	4 - 28		4 - 28	
H_s [m]	2.0		1.5	

To calculate the response spectrum, the wave spectrum is multiplied by the square of the RAO, as shown by equation 14, where $S_x(\omega)$ is the response spectrum, $S_w(\omega)$ is the wave spectrum and $H(\omega)$ is the RAO (Journée [2001]). Using the area under of the resulting response spectrum, the significant amplitudes are calculated. The significant amplitude can then be multiplied with 1.86 to get the most probable maximum motion amplitude in a 3 hour sea state.

$$S_x(\omega) = S_w(\omega) \times |H(\omega)|^2 \quad (14)$$

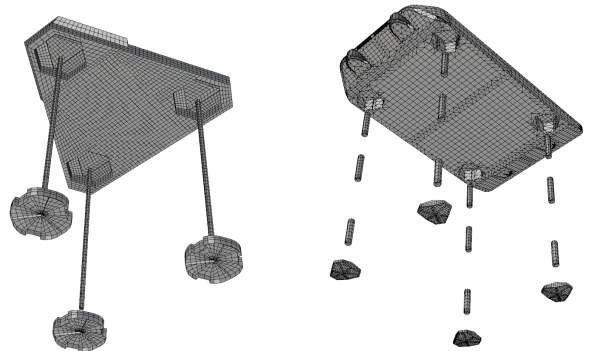


Figure 13: Panel models used in analysis. Left: CJ-70, right: NG-2500X

Figure 14 shows the resulting CoG Roll and spudcan heave RAO's of the CJ-70, and figure 15 shows the RAO's of the NG-2500X. The corresponding significant responses are shown by figures 16 and 17. Governing headings are 60° and 120° for the CJ-70 and NG-2500X respectively, where the waveward spudcans show the highest motion response (CJ-70: SB, NG-2500X: SB FWD). It is chosen to only show results for one water-depth per jack-up (CJ-70: 120[m], NG-2500X: 45[m]); results for other waterdepths are comparable.

⁴Existing, GustoMSC models of the CJ-70 and NG-2500X are used, made in Rhinoceros 5

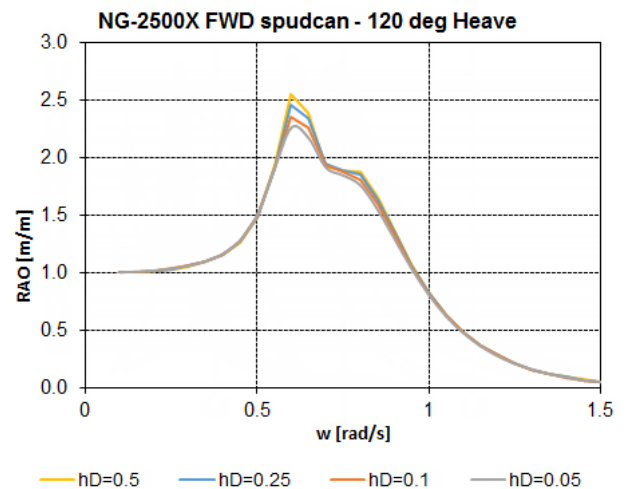
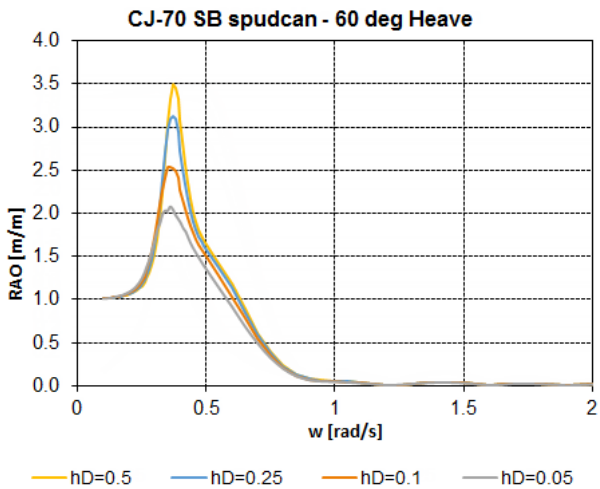
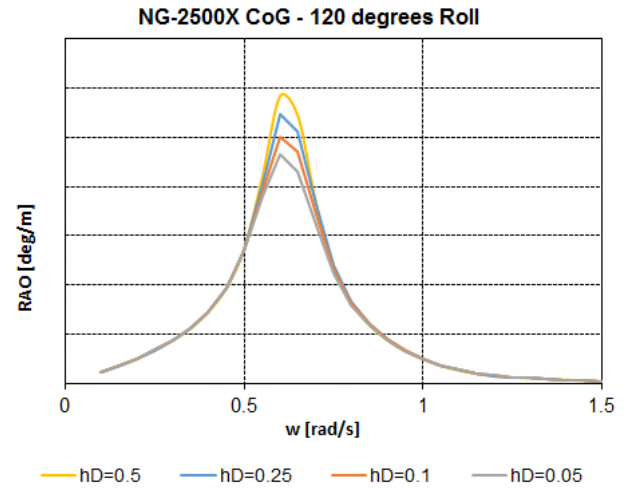
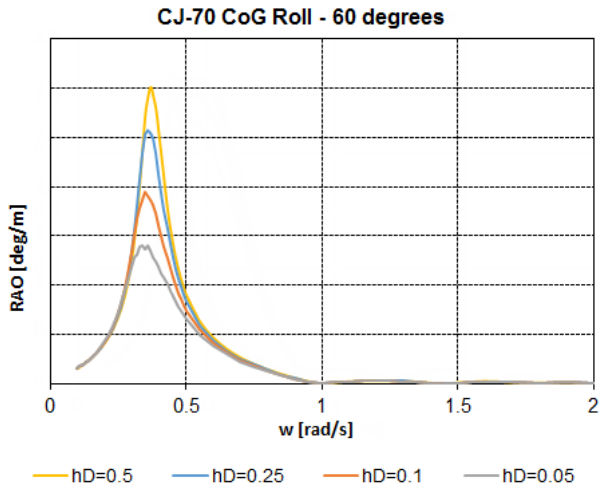


Figure 14: RAO CJ-70 - 120 [m] waterdepth

Figure 15: RAO NG-2500X - 45 [m] waterdepth

The CJ-70 has lower eigenfrequencies than the NG-2500X. The CoG of the CJ-70 has a roll and pitch eigenfrequency of $\omega_{n;roll} \approx 0.4$ and $\omega_{n;pitch} \approx 0.4$ [rad/s], respectively. For the NG-2500X CoG these are $\omega_{n;roll} \approx 0.6$ and $\omega_{n;pitch} \approx 0.8$ [rad/s]. The CJ-70 is mostly affected by long waves of $T_p \geq 11$ [s]. The NG-2500X is affected by shorter waves of $T_p \geq 7$ [s].

The biggest reductions of spudcan motions for decreasing $\frac{h}{D}$ are observed at the peaks of the RAO's and the peaks of the significant motion amplitudes (this is also true for surge and sway, which is not shown). This is an indication that the increase of C_d dampens the CoG motions at the respective eigenfrequencies and subsequently reduces the spudcan motions. For the CJ-70 this causes a significant reduction in the peaks of the spudcan RAO's (a reduction of over 40% for almost each direction and water depth). For the NG-2500X this effect is less pronounced (an average reduction of only 11% for each direction and water depth).

For the CJ-70, the significant amplitudes of the spudcan motions significantly decrease for sea states with a peak period range of $T_p \approx 11 - 25$ [s]. The significant amplitudes of the NG-2500X spudcan motions show a small decrease for sea states with the peak period range of $T_p \approx 7 - 15$ [s]. These reductions are within the impact governed period range. The distance of the spudcans to the seabed, $\frac{h}{D}$, should however be kept in mind when assessing the significant motion amplitudes. At $\frac{h}{D} = 0.05$, $h = 1.1$ [m] (CJ-70) and $h = 0.3$ [m] (NG-2500X). If $Z_s > h$ there will be a very large chance of impact and then the motions will be affected by more effects than hydrodynamics alone. The heave amplitude line then no longer has a defined physical meaning (showed by dotted lines).

For $\frac{h}{D} = 0.5$ to 0.05 , no significant shift in eigenfrequency can be observed. This is an indication that the increase in heave C_a of the spudcans does not have a significant effect on the motions. The reductions of the RAO's are significantly larger for the CJ-70 than for the NG-2500X hull. This is also true for the significant motion amplitudes.

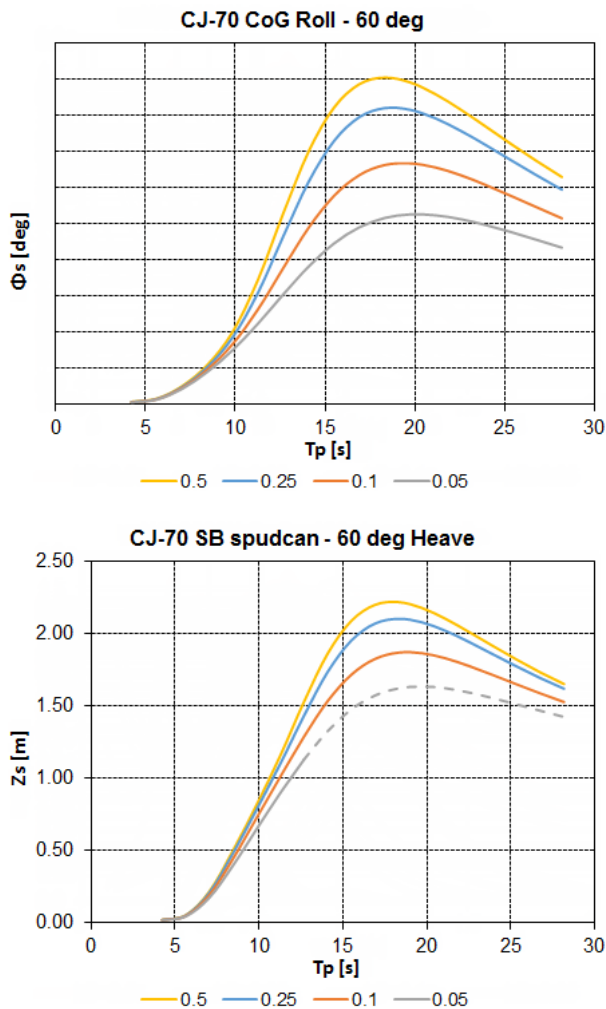


Figure 16: Significant amplitudes CJ-70 - 120 [m] water depth

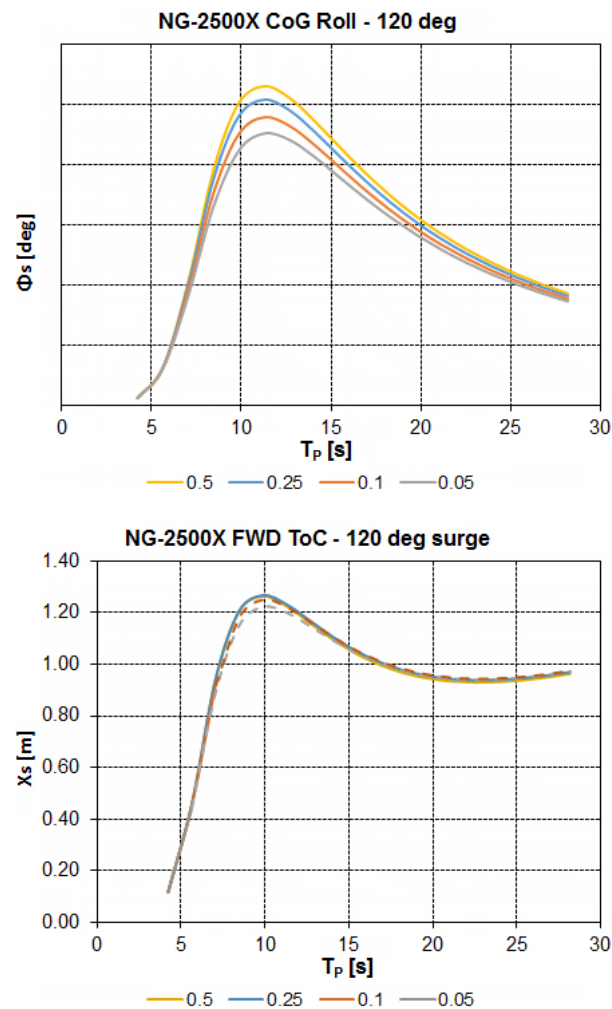


Figure 17: Significant amplitudes NG-2500X - 45 [m] water depth

5. Conclusions

The heave added mass coefficients, C_a , of both spudcan models increase with decreasing distance to the seabed and increase with increasing amplitude. The quadratic heave damping coefficient, C_d , increases with decreasing distance to the seabed and this increase is significantly larger for the skirted spudcan than for the hexagonal spudcan.

The increase of heave C_d causes the spudcan motions of the CJ-70 to significantly decrease in sea states with peak periods higher than 11[s], for decreasing distance between spudcans and the seabed. The spudcan motions of the NG-2500X showed a small decrease in sea states with peak periods higher than 7[s].

The found reductions are within the impact governed period range. Since spudcan impact loading is dependent on spudcan motions, a reduction of the significant motion amplitude in this area could indicate a reduction of spudcan impact loading.

This could subsequently lead to an improvement in calculated limiting environmental installation conditions in the impact governed period region.

For both typical jack-up's, it is not yet possible to quantify the improvement at this stage. For the CJ-70, however, the motion reductions are considered to be large enough to justify additional research into the actual reduction of the impact loads for large drilling jack-up's with skirted spudcans. In the authors opinion, the decrease of the NG-2500X motions are not significant enough, considering the current assumptions, to indicate a possible improvement of the calculated installation conditions for small wind turbine installation vessels, with hexagonal spudcans.

6. Recommendations

Further research is needed to analyze neglected effects and to quantify the possible improvement in calculated limiting environmental installation conditions, caused by the increased vertical drag force on the skirted spudcans.

It is recommended to:

- Perform time domain simulations to find the improvement of the motions when spudcan heave coefficients C_a and C_d are real-time dependent on the distance between spudcan and seabed. If the analysis method is able to combine hydrodynamics with a soil model, the change in impact loading and allowable installation sea states can be calculated.
- Investigate the influence of combined heave, surge and sway motions on the increase of heave coefficients C_a and C_d and is there a change of coefficients in the surge and sway directions. This can be done with additional model tests or CFD analyses.
- Investigate influence of realistic soil conditions on the increase of heave coefficients C_a and C_d . To analyze and define the soil influence will however be a challenge due to differences in scaling between soil and water.
- Investigate whether the post-processing method used for obtaining C_a and C_d from measured forces can be improved.

Symbols

z_0	Heave amplitude
$z(t)$	Vertical motion
\ddot{z}	Vertical acceleration
\dot{z}	Vertical velocity
$H(\omega)$	RAO
$S_w(\omega)$	Wave Spectrum
$S_x(\omega)$	Response Spectrum
β	Frequency parameter
μ	Dynamic viscosity
ν	Kinematic viscosity
ω	Frequency in [rad/s]
ϕ	Phase angle
ρ	Density of fluid
A	Added mass
A_{disk}	Theoretical heave added mass disk
B	Linearized damping
B_{pot}	Potential damping
$B_{visclin}$	Linearized viscous damping
C	Stiffness
C_a	Added mass coefficient
C_b	Linearized damping coefficient
C_d	Drag coefficient
D	Diameter
f	Frequency in [Hz]
$F(t)$	Force
$F_D(t)$	Damping force
h	Distance between spudcan and seabed
H_s	Significant Wave Height
KC	Keulegan-Carpenter number
M	Mass
r	Radius
Re	Reynolds Number
S	Area
T_p	Peak period

Abbreviations

CFD	Computational Fluid Dynamics
CoG	Center of Gravity
DoF	Degrees of Freedom
DP	Dynamic Positioning
DUT	Delft University of Technology
FWD	Forward
PM	Pierson-Moskowitz Spectrum
RMS	Root Mean Square Error
SB	Starboard

References

- C.E. Brennen. A Review of Added Mass and Fluid Inertial Forces, 1982.
- P. Chakrabarti. Going on Location Study for a Jack-Up Rig. In *OMAE*, Houston, 2012.
- DNV. DNV-RP-C104 Recommended practice Self-elevating Units, 2012.
- C. A. Garrido-mendoza, A. Souto-iglesias, and K.P. Thiagarajan. Numerical Simulation of Hydrodynamics of a Circular Disk Oscillating Near a Seabed. In *OMAE*, Nantes, 2013.
- C.A. Garrido-Mendoza and K.P. Thiagarajan. Numerical Investigation of the Flow Features around Heave Plates Oscillating Close to a Free Surface or Seabed. In *OMAE*, San Francisco, 2014.
- H. He, A.W. Troesch, and M. Perlin. Hydrodynamics of damping plates at small KC numbers. In *IUTAM Symposium on Fluid-Structure Interaction in Ocean Engineering*, 2008.
- S. F. Hoerner. *Fluid-Dynamic Drag*. 1965.
- J. Ireland. Investigation into the sensitivity of the dynamic hook load during subsea deployment of a suction can. In *OMAE*, San-Diego, 2007.
- J.M.J Journée. *Offshore Hydromechanics*. Delft, 2001.
- H. Lamb. *Hydrodynamics*. New York, 1932.
- J. Li, S. Liu, M. Zhao, and B. Teng. Experimental Investigation of the Hydrodynamic Characteristics of Heave Plates Using Forced Oscillation. *Ocean Engineering*, 66, 2013.
- MathWorks. Evaluating Goodness of Fit, 2015. URL <http://nl.mathworks.com/>.
- B. Molin, P. Guérin, D. Martigny, and P. Weber. Etude Theorique et Experimentale des Efforts Hydrodynamiques sur une Embase Plane a l'Approche du Fond Marin. In *7e Journees de l'Hydrodynamique*, Marseille, 1999.
- F. Nielsen and Statoil. How to Estimate Hydrodynamic Coefficients Applicable for Lifting From the Seabed, 2007.
- O. A. J. Peters and R. H. M. Huijsmans. Assessing Hydrodynamic Behavior During Offshore Loading and Discharge in the Heavy Marine Transport. In *OMAE*, Rotterdam, 2011.
- T.F. Roe. Heave Added Mass and Damping of a Suction Can in Proximity to the Sea Floor. In *OMAE*, Estoril, 2008.
- T. Sarpkaya and M. Isaacson. *Mechanics of Wave Forces on Offshore Structures*. New York, 1981.
- L. Tao and D. Dray. Hydrodynamic Performance of Solid and Porous Heave Plates. *Ocean Engineering*, 35, 2008.

- L. Tao and K.P. Thiagarajan. Low KC Flow Regimes of Oscillating Sharp Edges. II. Hydrodynamic forces. *Applied Ocean Research*, 25, 2003a.
- L. Tao and K.P. Thiagarajan. Low KC Flow Regimes of Oscillating Sharp Edges I. Vortex Shedding Observation. *Applied Ocean Research*, 25, 2003b.
- H. Wadhwa. Variation of Heave Added Mass and Damping Near Seabed. In *OMAE*, Shanghai, 2010.
- J. Yang, X. Tian, and X. Li. Hydrodynamic characteristics of an oscillating circular disk under steady in-plane current conditions. *Ocean Engineering*, 75, 2013.